Prelaunch Performance of the NASA Altimeter for the TOPEX/POSEIDON Project

Paul C. Marth, J. Robert Jensen, Charles C. Kilgus, James A. Perschy, John L. MacArthur, David W. Hancock, George S. Hayne, Craig L. Purdy, Laurence C. Rossi, and Chester J. Koblinsky

***Abstract*—Validation of in-orbit performance has demonstrated the ability of satellite radar altimetry to measure mesoscale absolute dynamic sea surface topography and to measure the variation in the general circulation on the largest spatial scales. Measurements of basin scale mean circulation, however, have been corrupted by system inaccuracies. The TOPEX/POSEIDON radar altimeter satellite applies recent advances in remote sensing instrumentation to reduce long wavelength measurement errors to dramatically lower levels. The TOPEX altimeter measures the range to the ocean surface with 2-cm precision and accuracy through the use of both *Ku*- and *C*-band radars, a high pulse repetition frequency, an agile tracker, and absolute internal height calibration. Dual pulse bandwidths for both frequencies make it possible to quickly acquire the surface and begin tracking after crossing the land/ocean boundary. This paper presents the altimeter requirements and the elements of the altimeter design that have resulted in meeting these requirements. Prelaunch test data, based on the use of a Radar Altimeter System Evaluator to simulate the backscatter from the ocean surface, are presented to demonstrate that the TOPEX altimeter will meet these requirements and provide the data necessary to the understanding of basin scale mean circulation.**

Nomenclature

AGC	Automatic Gain Control
AGC Gate (G_{AGC})	Average of 32 waveform samples centered on the ocean return leading edge. Used to set the receive AGC such that this gate is maintained at a predetermined level.
AXBT	Air Expendable Bathythermographs
Burst	Pattern of transmit/receive periods or gates with fixed timing as illustrated in Fig. 5. The interburst gap varies with height to maintain the ocean return receive periods fixed relative to the transmit periods. The returns from six bursts are accumulated for updating the height, height rate, Ku/C height difference, AGC, SWH, etc. There are 38 *Ku*-band and 10 *C*-band transmit/receive periods per burst.
CSSA	*C*-band Solid State Amplifier
Early Gate (G_E)	Formed from a group of waveform samples positioned on the "early" portion of the ocean return leading edge. Used in conjunction with the "Late Gate" primarily for estimation of leading edge slope for SWH determination. The number of waveform samples used to form this gate is a function of the "gate index."
EMI/EMC	Electro-Magnetic Interference/Electro-Magnetic Compatibility
f^2	Frequency squared (*Ku*- or *C*-band)
FFT	Fast Fourier Transform
FM	Frequency Modulation
Gate	Average of a contiguous set of waveform samples used for height tracking, AGC, SWH determination, etc. Refer to Table II and Fig. 6 for the definition of the various waveform sample gates used by the altimeter.
Gate Index	Index with a range of 1 to 5 derived by examination of each "Early/Late" gate pair to determine which pair provides the best fit to the ocean return leading edge waveform.
GSFC	Goddard Space Flight Center
h	Height (*Ku*- or *C*-band)
Δh	Height error
JHU/APL	The Johns Hopkins University/Applied Physics Laboratory
Late Gate (G_L)	Formed from a group of waveform samples positioned on the "late" or "plateau" portion of the ocean return leading edge. Used in conjunction with the "Early Gate" primarily for estimation of leading edge slope for SWH determination. The number of waveform samples used to form this gate is a function of the "gate index."
LVPS	Low Voltage Power Supply
M	Number of waveform samples used to compute the Middle gate [refer to Eq. (14) and Table IV].

Manuscript received July 15, 1992; revised November 13, 1992.

P. C. Marth, J. R. Jensen, C. C. Kilgus, J. A. Perschy, and J. L. MacArthur are with the Johns Hopkins University, Applied Physics Laboratory, Laurel, MD.

D. W. Hancock, G. S. Hayne, C. L. Purdy, and L. C. Rossi are with the NASA Goddard Space Flight Center, Wallops Flight Facility, Wallops Island, VA.

C. J. Koblinsky is with the NASA Goddard Space Flight Center, Greenbelt, MD.

IEEE Log Number 9206928.

Middle Gate (G_M)	Formed from a group of waveform samples positioned on the "middle" portion of the ocean return leading edge. Used in conjunction with the "AGC" and "Noise" gates for estimation of height error. The number of waveform samples used to form this gate is a function of the "gate index."
NASA	National Aeronautics and Space Administration
N_{eff}	Effective number of independent pulses in a 3-s interval [refer to Eq. (14) and Table IV].
Noise Gate (G_N)	Average of four waveform samples prior to ocean return leading edge used to estimate background noise floor in the waveform samples (refer to Table II and Fig. 6).
ONA	Off-Nadir Angle
POCC	Program Operations Control Center
PRF	Pulse Repetition Frequency which is a function of altitude.
r	Height Rate
RASE	Radar Altimeter System Evaluator (i.e., equipment used to test the altimeter and assess its performance).
RSS	Return Signal Simulator (part of RASE)
σ	Radar Cross-section (m^2)
S	Slope (of ocean return leading edge)
SNR	Signal-to-Noise Ratio
std	Standard Deviation
SWH	Significant Wave Height ($H_{1/3}$) is defined as the average of the highest third of the waves in the wave record.
SYNOP	Synoptic Ocean Prediction
Sigma-Zero (σ^0)	Ocean Backscatter coefficient in dB
τ	Pulse width 102.4 μs (uncompressed), 3.125 μsec (compressed) or Track Interval (nominally 53 ms)
TECU	Total Electron Count Unit (free electrons/m^2)
TWTA	Travelling Wave Tube Amplifier
Tracker Interval	Period over which ocean returns are gathered for updating the estimation of height, height rate, Ku/C height difference, SWH, AGC, etc. (equal to six bursts and is a function of altitude, nominally 53 ms).
UCFM	Up-Converter Frequency Multiplier unit
var	Variance
Waveform Sample	Ocean return power detected in a single or group of range bins (one bin resolution is 0.47 m when using the 320 MHz transmission bandwidth) summed over a number of pulse returns (e.g., 228 *Ku*-band and 60 *C*-band for one track update interval). There are 128 single waveform samples developed for the ocean return for each track interval of 6 "bursts." These are averaged and compressed into 64 samples for inclusion in the altimeter telemetry output.

I. Introduction

THE earth provides mankind a thin blanket of air, a thinner film of water, and the thinnest veneer of soil to support the daily needs of more than five billion people. Catastrophic changes that humans have made in the local environment, e.g., in the ecosystems of our rivers, bays, and near-shore ocean areas, are now taken for granted. Concern is increasing that the Earth's global environment may also be changing in ways to which we may not easily adjust.

The ocean circulation is a dominant element of this global climate system, one of the working fluids in the heat engine that transports heat from the equatorial tropical zone to the polar regions. Change in the circulation is simultaneously both the cause of and indicator of climatic change. Changes in this global fluid have global consequences (climate) as well as regional ones (weather, fisheries, military and commercial operations, etc.). The circulation spatial scales of interest, therefore, range from the mesoscale (of order 100 km) to basin scale (of order 10 000 km). Temporal scales of interest vary from the yearly variations in the time averaged, large scale mean circulation to monthly (or even weekly) variations in the energetic, small scale, time-dependent processes that are superimposed on the mean fields.

The length and time scales of these processes are too large for conventional oceanographic instrumentation. Even regions of comparatively modest size, a few hundred kilometers across, cannot be adequately measured by shipboard or moored instruments. Satellite altimetry is the only known method by which oceanographers can precisely and accurately measure sea surface topography. The shape of the sea surface is the only physical variable measurable from space that is directly and simply connected to the large scale movement of water and the total mass and volume of the ocean [1].

The fundamental altimetric concept for measuring the ocean circulation is simple. Movement of water in the sea on spatial scales exceeding about 30 km and temporal scales exceeding about 1 day are manifested by deflections of the sea surface; that is, by changes in mean sea level associated with the strength and direction of the flow. This change in topography varies from the 1-meter increase in mean sea level in 100 km over the Gulf Stream to a 10 cm change over 1000 km over an El Nino event in the tropical Pacific. Given the strength of the sea surface topography signature, one can infer the magnitude and direction of the oceanic water movement. The sea surface elevation changes measured by the altimeter reflect more than just surface conditions. Hydrodynamics show that a sea surface topography change over 500 km reflects oceanic currents to depths of 500 to 1000 m.

Fig. 1. An estimate of the large-scale global surface topography and circulation of the ocean relative to the geoid based on 2 years of GEOSAT altimeter measurements.

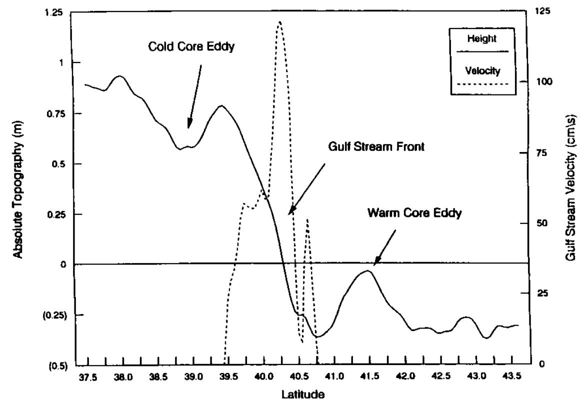

Fig. 2. A profile of GEOSAT absolute topography and Gulf Stream velocity over the SYNOP array on April 21, 1988.

The altimeter instrument is conceptually simple; a nadir looking, high-resolution radar that measures the distance from the satellite to the ocean's surface with an accuracy of a few centimeters. This range measurement combined with precise knowledge of the satellite orbit, propagation effects, and the earth's geopotential field (the surface of no motion) provides a measure of sea height above the geoid. A time history of altimeter data then provides a profile of sea surface topography along the satellite subtrack. A first estimate of basin scale topography and circulation based on GEOSAT data [1] indicates the potential for global ocean monitoring (Fig. 1).

A. Past Achievements in Altimetry

Extensive data validation programs have demonstrated the capability of past radar altimeter missions (GEOS-3, SEASAT, GEOSAT) to: measure the dynamic topography of the Western Boundary currents and their associated rings and eddies [2], [3]; determine the absolute circulation of the ocean gyres [4]–[7]; estimate variation of the circulation on the very largest spatial scales [8]–[10]; provide global mapping of eddy energies [11]–[16]; measure fluctuations in the great current systems [17], [18]; and provide altimeter data for assimilation into numerical models [19]–[24]. Descriptions of the GEOSAT system characteristics were collected in two special issues of the *JHU/APL Technical Digest* [25], [26]. Extensive references and collections of ocean science results were presented in the special issues of the *Journal of Geophysical Research* on GEOS [27], SEASAT [28], [29], and GEOSAT [30], [31].

As a typical example of altimetric measurements of the Western Boundary currents, absolute dynamic topography and current velocity were computed for the ascending GEOSAT passes over the Synoptic Ocean Prediction (SYNOP) array in the Gulf Stream of April 21, 1988 [32]. The data (Fig. 2) show the position of the Gulf Stream axis at 40.31°N with a maximum velocity of 122 cm/s. In addition, there are cold and warm core eddies centered at 38.9°N and 41.6°N, respectively. During the SYNOP experiment, there was an aircraft underflight of a GEOSAT pass on June 12, 1988 during which Air Expendable Bathythermographs (AXBT's) were dropped. Comparison of the absolute topography from the altimeter and AXBT's shows an rms difference between these two methods of 6.8 cm. The altimeter profile was processed with a "synthetic geoid" that provides a precise surface of no motion at mesoscale wavelengths [33]–[37].

Although dramatic results have been achieved, past altimetric missions were not designed for the purpose of understanding global change. The absolute mesoscale wavelength topography agreement shown for GEOSAT is possible only because the variations in the residual errors in the orbit determination, radio propagation, and synthetic geoid corrections are predominantly at long wavelengths. Measurements of basin scale mean circulation were corrupted by system inaccuracies. The circulation measurements needed for monitoring climate change will require that the basin scale errors be reduced to the few centimeter level.

B. The TOPEX/POSEIDON Altimeter Mission

The TOPEX Science Working Group [38] concluded in 1981 that, based on SEASAT data, the basin scale mean circulation of the ocean could be measured with a radar altimeter satellite if advances in remote sensing instruments and in ocean science allowed long wavelength measurement errors (altimeter noise and drift, ionospheric and water vapor propagation, orbit determination, tide models, geoid models, and electromagnetic bias) to be reduced to dramatically lower levels. A radar altimeter was required with 2 cm absolute long-term calibration that would measure the range to the ocean's surface with a few centimeters precision despite ionospheric error.

The ionosphere directly impacts the altimeter measurement by lengthening the electromagnetic path to the surface in proportion to the total electron content along the path. Since the delay is inversely proportional to frequency squared, an

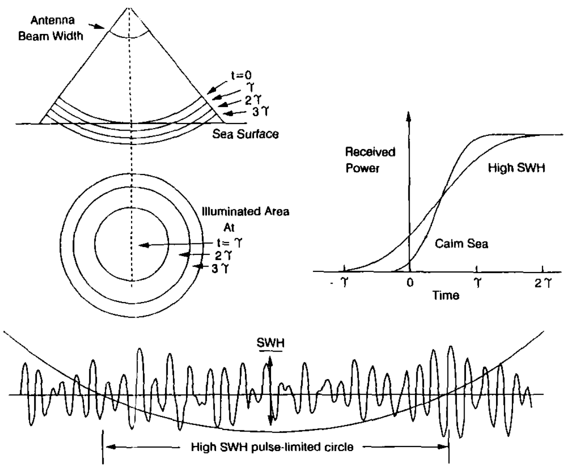

Fig. 3. Altimeter pulse limited measurement geometry.

altimeter that measures height at two frequencies allows the error to be corrected.

During the 11 years since the science report, the required NASA radar altimeter has been developed and is now integrated with the TOPEX/POSEIDON satellite in anticipation of launch.

This paper describes the system design characteristics of the altimeter that directly impact the measurement performance and provides prelaunch test data establishing the capability of the instrument. Companion papers describe the predicted ionospheric height correction precision possible with the altimeter [39] and describe the prelaunch state of knowledge in precision orbit determination [40], electromagnetic bias [41], tide models [42], and geoid models [43].

C. Measurement Geometry and Return Waveform

The characteristics of a signal reflected from the ocean surface strongly influence an altimeter's design and impose limits on the precision attainable, even for a perfect instrument [44], [45]. A pulse-limited mode of operation is used in which the intersection of a spherical shell (representing the locus of points equidistant from the radar) with the ocean's surface defines regions where the lateral extent is small compared with that defined by the antenna beamwidth. That is, the surface area corresponding to the range resolution of the altimeter is much smaller than that encompassed by the antenna beam (Fig. 3).

The earliest signal returns come from wave crests. Reflecting facets deeper in the waves then gradually contribute, accompanied by an increase in the illuminated area within a range resolution cell until a point is reached where the surface of constant range reaches the wave troughs. Beyond that point, the illuminated area within a range resolution cell remains essentially constant. The signal amplitude would also remain constant, except for the antenna pattern attenuation that imparts a decay in amplitude that is exponential for a nadir pointing antenna and more complicated but calculable for off-nadir pointing. The result is a waveform whose average shape is given by the double convolution of the system's point target response, the ocean-surface height distribution, and the calm-sea impulse response (essentially, a step function modulated by a two-way antenna pattern). The antenna beamwidths are much smaller than Fig. 3 suggests (less than 1°); thus, the variation of surface reflectivity with incidence angle is neglected.

The sharply rising leading edge of the waveform is the basis for the precise height estimation. The half-power point conforms closely to mean sea level. The instrument tracks the location of that point with respect to the transmitted pulse, and the height measurement is telemetered to the ground. The slope of the leading edge provides a measure of ocean wave height but also results in degraded measurement precision with increasing wave height. This degradation is counteracted in part by adaptively increasing the width of the tracking gate that senses the location of the leading edge. The addition of adjacent high-resolution samples to form a wider gate leads to a reduction in noise.

As part of the overall height and wave-height estimation process, the amplitude of the ocean-return signal is normalized via an automatic gain control (AGC) loop. Properly calibrated, the AGC setting is a measure of the backscatter coefficient at the surface that, in turn, depends on wind speed.

D. NASA TOPEX Altimeter Functional Description

The NASA TOPEX altimeter functions as a dual frequency, nadir-looking, pulse-compression radar. The range measurements at both *Ku*-band (13.6 GHz) and *C*-band (5.3 GHz) allow compensation for the range delay/error resulting from ionospheric electron content.

The system generates a linear-FM (chirp) pulse waveform with a bandwidth of 320 MHz and a duration of 102.4 μs for both *Ku*- and *C*-band. The pulse repetition frequency (PRF) of the *Ku*-band channel is approximately 4500 Hz, while the PRF of the *C*-band channel is approximately 1200 Hz.

The antenna is a 1.5 m diameter parabolic reflector. The beamwidth (1.1° for *Ku*-band) of this antenna covers an area on the surface that has a diameter of over 20 km. The measurement area is restricted by the pulse-limited operation to an area of 2 km for a flat sea surface or 7 km for a 5 m significant wave height (SWH) surface.

The received pulses are deramped to remove the linear-FM and processed by frequency filtering to form waveforms, each consisting of 128 samples of the power backscattered from a particular range. The 320 MHz pulse bandwidth results in these samples having a spacing of 0.47 m. The ultimate resolution of the altimeter is achieved by effectively interpolating between the sampled waveform points. The waveforms are processed by an adaptive tracker, which uses an Intel 80186 microprocessor. The tracker controls the altimeter through the various calibrate, track, standby, and test modes in response to commands received via the spacecraft command link. It formats the height, AGC, wave height, status, and engineering data for output to the spacecraft telemetry system.

The dual frequency high PRF transmitted waveform is a critical performance driver and is described later. The major characteristics of the altimeter are listed in Table I. A complete description of the altimeter is available elsewhere [46].

TABLE I
NASA TOPEX ALTIMETER CHARACTERISTICS

	Ku-Band	Common	C-Band
Mean Altitude (km)		1334	
Frequency (GHz)	13.6		5.2
Peak RF Power (W)	20.0		20.0
Antenna Diameter (m)		1.5	
Beam Width (Deg)	1.1		2.7
Gain (dB)	43		36
Pulse Width (Microsec)	102.4		102.4
Bandwidth (MHz)	320,5		320, 100,5
Pulse Rate (Hz)	4500		1200
Weight (lb)		480*	
Power (W)		234	
Attitude Control (Deg)		0.42	
Science Data Rate (kb/s)		10	
Microprocessor		Intel	

*Includes antenna

E. Fundamental Determinants of TOPEX Altimeter Performance

Measuring mean ocean circulation imposes unique requirements on the TOPEX altimeter that cause its performance to be significantly improved over previous altimeters [47]:

1) Correction for ionospheric path delay: The altimeter provides ≤ 2.4 cm height error (3 s average, 2 m significant wave height) despite the variation in ionospheric path delay. This is accomplished by measuring the range to the surface at both *Ku*- and *C*-band.

2) Height error at high sea states: The specified height error in the combined Ku/C-band measurement varies with SWH as follows:

$$\begin{aligned}\text{Height error } &\leq 1.7 \text{ cm for 2 m SWH}\\ &\leq 2.1 \text{ cm for 4 m SWH}\\ &\leq 3.0 \text{ cm for 8 m SWH}\end{aligned}$$

This is accomplished by a high PRF waveform design that takes advantage of the available pulse-to-pulse independence at high wave heights, thus delivering improved height noise at high sea states compared to previous altimeters.

3) Tracker signal-to-noise ratio (SNR) at 1334 km: The 13 dB minimum received SNR is maintained despite the TOPEX satellite altitude of 1334 km. This is accomplished through the use of a 1.5 m diameter, focal-point-fed parabolic antenna aperture.

4) Range tracking agility: The range error is maintained below 1.7 cm for 2 m SWH despite a height rate of up to 50 m/s and height acceleration of 1 m/s^2.

5) Absolute internal height calibration: The initial height bias is determined within 1.5 cm in ground testing and the height drift is correctable to ≤ 2 cm per 10-day period after appropriate calibrations. This is accomplished by implementing a dual-frequency internal calibration loop that is used to periodically measure height calibration drift in orbit. It employs the "full deramp chirp" height measurement technique that is insensitive to temperature effects.

6) Dual-resolution surface acquisition: It is predicted that all performance parameters will be met in orbit within 5 s of crossing a land/ocean boundary. This is accomplished with the use of a separate coarse resolution acquisition chirp waveform.

7) Dual Frequency Prelaunch Performance Validation: The performance of the altimeter is validated over the range of in-orbit operating conditions before launch. This is accomplished with a Radar Altimeter System Evaluator that provides a full dual frequency simulation of the ocean surface.

8) Three-year design lifetime: Long instrument life is required to measure the variation in the mean circulation. This is accomplished by a completely redundant altimeter that provides two parallel independent instruments that share a common antenna.

II. ALTIMETER SYSTEM OPERATION

The TOPEX altimeter is designed such that many of the details of operation can be modified by uploading new parameters into the adaptive tracker unit memory. The following discussion is based on those parameters stored in read-only-memory and designed for initial use.

A. TOPEX Altimeter Signal Flow

The TOPEX altimeter operation will normally involve a sequence of several modes that include acquisition and tracking at low resolution, and two calibration modes. In the following discussion, only high-resolution tracking will be addressed. This mode produces height measurements that are useful to the study of ocean topography. The remaining modes serve to initiate high-resolution tracking and to aid in the interpretation of the measured absolute heights. The time required for the acquisition of the surface and the establishment of tracking will be discussed later.

The TOPEX block diagram is shown in Fig. 4. As stated above, the TOPEX altimeter transmits 102.4 μs-long pulses with a 320 MHz bandwidth for both *Ku*- and *C*-band. The pulses are linear-FM modulated with a decreasing frequency. This pulse format and the development of the *Ku*-band signals described below are the same as used for the GEOSAT-1 altimeter with a time-bandwidth product of 32768. This yields a compressed pulse of 3.125 μs which is identical to the SEASAT-1 altimeter which employed a 3.2 μs, 320 MHz bandwidth linear-FM format (i.e., a 1024 time-bandwidth product). The longer duration pulse, 102.4 μs, used for TOPEX and GEOSAT permitted reduction of the peak transmitted power from 2 kW (SEASAT) to 20 W without compromising SNR.

The pulses are created within the two sections of the chirp generator. The digital section uses direct digital synthesis to achieve a full length pulse at baseband with a 40 MHz bandwidth. The RF section converts the digital inphase and quadrature signals to analog signals, mixes these with a 125 MHz carrier, then performs a frequency doubling to obtain a 80 MHz bandwidth pulse on a 250 MHz carrier.

An upconverter module mixes these pulses with 3150 MHz and frequency-multiples by a factor of 4 to obtain full 320 MHz *Ku*-band pulses with a center frequency of 13.6 GHz. In addition, a pulse is generated with full bandwidth at a center frequency of 13.1 GHz by mixing with 3025 MHz

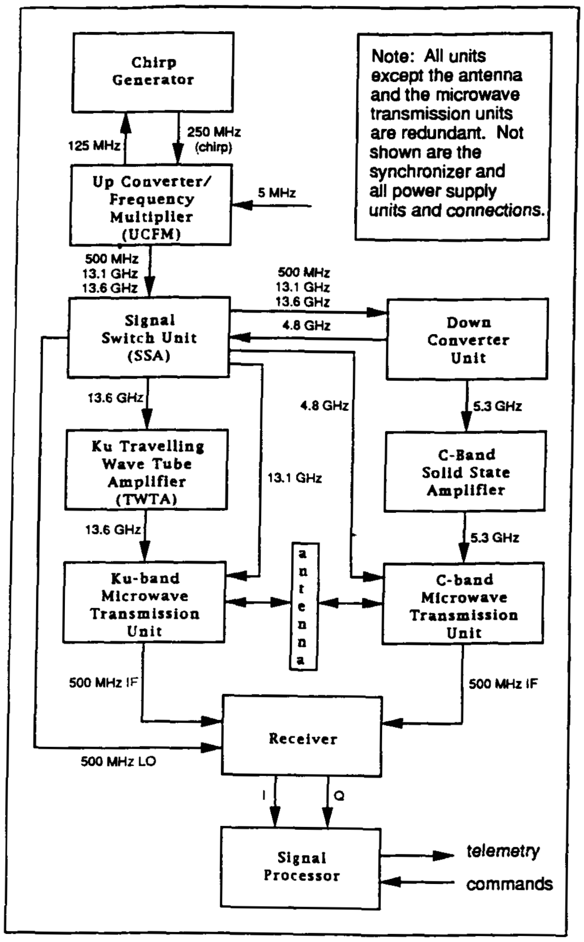

Fig. 4. Block diagram for NASA TOPEX altimeter. Only half of the fully redundant altimeter is shown. The full altimeter consists of independent "A" and "B" sides. The only elements common to both sides are the microwave transmission units and the antenna.

in place of 3150 MHz. This will be used as the local oscillator (l.o.) signal in the receiver.

A downconverter module produces the C-band pulses by mixing the Ku-band pulses with a 8300 MHz CW signal and produces center frequencies of 5.3 and 4.8 GHz. These are the transmit pulse and the l.o. pulse, respectively.

The Ku-band pulses are amplified to 20 W of peak power by a traveling wave tube (TWT). The C-band pulses are also amplified to 20 W of peak power, but in this case a solid state amplifier is employed. Both pulses are transmitted through a common 1.5 m parabolic antenna.

The transmission timing is shown in Fig. 5. Transmission occurs in "bursts." Each burst consists of 38 Ku-band pulses and 10 C-band pulses. Every other burst begins with the transmission of a Ku-band pulse and simultaneous reception of a C-band pulse. Following this is a 5 μs guard interval and then reception of a Ku-band pulse and transmission of a C-band pulse. For Ku-band, this alternating transmission and reception continues throughout the burst. For C-band, six pulse

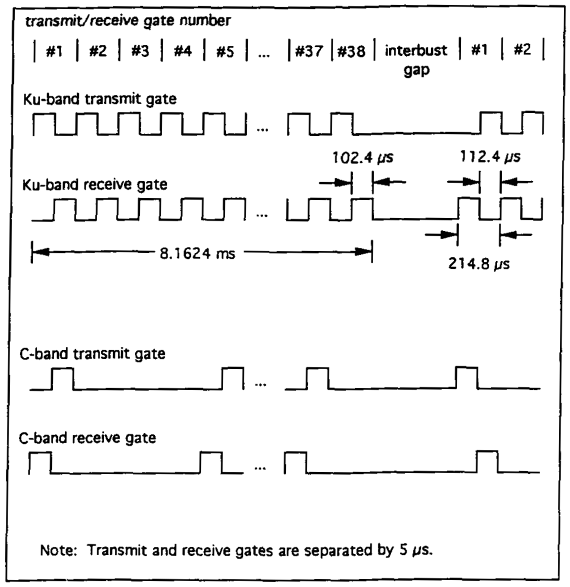

Fig. 5. Transmit and receive gate timing diagram for the NASA TOPEX altimeter. This diagram assumes that the Ku-band channel is the primary channel and that the altimeter is operating in high resolution mode. The length of the interburst gap is variable and depends on the altimeter height. The pulses within the 8.1624 ms interval constitute one burst. A burst contains 38 Ku-band pulses and 10 C-band pulses.

intervals elapse before the next reception–transmission pair occurs. This results in the C-band PRF being one-fourth of the Ku-band PRF during the burst. On the next burst, the transmit and receive operations are reversed for both bands.

The burst configuration maximizes the number of pulses per "track interval," the update period for the ocean return tracking process (six bursts), which is variable with altitude, but nominally 53 ms. This is discussed in more detail later. For comparison, the GEOSAT and SEASAT altimeters had 50 pulse returns per track interval (50 ms) whereas TOPEX with the burst format receives 228 Ku-band and 60 C-band returns.

The pulses per burst are less for the C-band channel to allow a pulse duty-cycle, about 10%, which is within the capability of solid-state implementation for a 20 W peak pulse power. (The Ku channel has a duty-cycle close to 50% and employs a TWT which is capable of CW at 20 W.) The lower duty-cycle of the C-band channel is compensated by the fact that in determining the resultant height from the Ku- and C-band measurements, the C-band data are de-weighted by a factor of 0.18 [refer to Eq. (15) of Section C].

The timing of events within a burst is fixed. The transmit/receive gates are 102.4 μs long and begin at 107.4 μs intervals. The interval between the beginning of one burst and the beginning of the next burst is variable and depends on the measured altitude of the satellite. For the nominal altitude of 1334 km, the bursts start at 8.9 ms intervals. For the range of altitudes of 1274 to 1394 km, the intervals range from 8.5 ms to 9.3 ms.

All pulse timing is based on an 80 MHz clock signal. The smallest variation of this timing is therefore 12.5 ns. This corresponds to a height change of 1.875 m. The burst timing is common to both altimeter frequencies. Finer adjustments of height are accomplished within the signal processor, as will be discussed below.

The received pulses are amplified and then mixed with the l.o. pulse to produce a signal roughly centered at 500 MHz with a bandwidth of 2 or 3 MHz. The spectral shape of this signal contains the information of interest about the ocean surface. The l.o. pulse is a replica of the transmitted pulse that is lower in frequency by 500 MHz. This process is described in more detail in [44].

The dechirped signal is then mixed down to inphase and quadrature video signals, filtered with a 625 kHz lowpass filter, and digitized at a 1.25 MHz rate. The bandpass filter eliminates high frequency components of the returned pulse that would otherwise be aliased into the signal band. These higher frequency components result from backscatter that occurs well away from the nadir point and are not of interest to height determination.

At the 1.25 MHz sample rate, the 102.4 μs pulse results in 128 complex samples. Before further processing, a frequency shift is applied to these digital samples. This shift accomplishes the fine adjustment of the altimeter height. Because of the nature of the linear-FM pulse, a small frequency shift has approximately the same effect as a time shift. This frequency shift accounts for height adjustments smaller than the 12.5 ns resolution of the receive gate timing. If only one channel was used, then the receiver gate timing could be chosen to be within 6.25 ns of the desired value. The need to accommodate two channels and a height rate as large as 50 m/s results in the receiver gate being as much as 12.5 ns from the desired value. This requires a frequency shift of as much as ± 39.0625 kHz.

The frequency shifted values are Fourier transformed within a digital filter bank. The square magnitude of the complex Fourier transform is computed. This represents the waveform for one altimeter pulse. Each point on this waveform can be interpreted as the amount of power reflected back to the altimeter from a given range interval.

The dominant noise source is speckle noise. This speckle results from the fact that the fields scattered back to the altimeter from the ocean surface are the coherent sum of backscatter from many, independently phased facets. The mean backscattered power is the sum of the power from the individual facets due to the random phases. At a given instant, however, the power may be greater or less than the mean depending on whether facets add constructively or destructively. As a result of the central limit theorem, the predetected waveforms will have a Gaussian amplitude distribution and hence the power is expected to have a negative exponential distribution with a standard deviation that is equal to the mean. We therefore have little confidence in the waveform values determined from a single pulse.

The waveforms also include a white noise floor that results from thermal noise in the first stage of amplification in the receiver. The importance of this noise will depend on the power of the transmitted signal, the antenna gain, the reflectivity of the ocean surface, and other factors in the link equation. The speckle noise statistics, however, depend on none of these factors and are independent of the altimeter design or application.

TABLE II
DEFINITION OF EARLY, MIDDLE, AND LATE GATES FOR GATE INDEXES 1 THROUGH 6

Gate Index	Early Gate	Middle Gate	Late Gate
1	32	32-33	33
2	31-32	32-33	33-34
3	30-31	31-34	34-35
4	27-30	29-36	35-38
5	21-28	25-40	37-44
6	9-24	Not Used	41-56

Each gate is the average of the waveform samples shown in the table. Early and late gates for index 6 are used to estimate the significant wave height of the surface. The noise gate is waveform samples 5–8. The AGC gate is samples 17–48.

To minimize the impact of the noise in the height measurement, the waveforms from many pulses are averaged together to form a single "tracker" waveform. Six bursts are grouped together to form what is referred to as one "track interval." This corresponds to 228 pulses for *Ku*-band and 60 pulses for *C*-band. One track interval corresponds to about 53 ms of data. This is the smallest time scale on which the signal processor interprets the waveforms.

Interpretation of the waveforms involves the operation of several feedback loops. The signal processor attempts to maintain a fixed difference between the waveform noise floor and the plateau height of the waveform. This is done by measuring this difference and adjusting the value of an attenuator so as to achieve the desired value. The processor also attempts to maintain a fixed position of the waveform. This is done by determining the present position of the waveform leading edge and adjusting the timing of the bursts and the value of the frequency shift in the digital filter bank. Both of these operations are based on the application of a set of "gates" to the waveform. These gates are referred to as the noise gate, the AGC gate, and the Early, Middle, and Late gates. Each gate is the average value of the waveform within a set of contiguous waveform values. The waveform samples constituting each gate are defined in Table II and are shown in Fig. 6 relative to a typical ocean return waveform. Waveform sample 1 represents the earliest returned power, and waveform 128 represents the latest. The surface leading edge is maintained at sample 32.5.

The noise gate is the average of waveform samples 5 through 8. The value of this gate is used to estimate the white noise floor in the waveform. Waveform samples 1 through 4 are not used due to the frequency shift that occurs within the digital filter bank. The maximum frequency shift corresponds to a time shift of 12.5 ns, which is four filter bins. This shift may result in high frequency components of the received pulse being "wrapped around" into the low frequency waveform samples. For that reason, the first four samples are avoided.

The AGC gate is the average of waveform samples 17 through 48. These samples are centered around waveform sample 32.5, which is the desired track point. The noise gate value is subtracted from the AGC gate to formulate an estimate of the return signal level. The signal processor maintains the value of the AGC gate at a specified value by adjusting attenuators in the receiver.

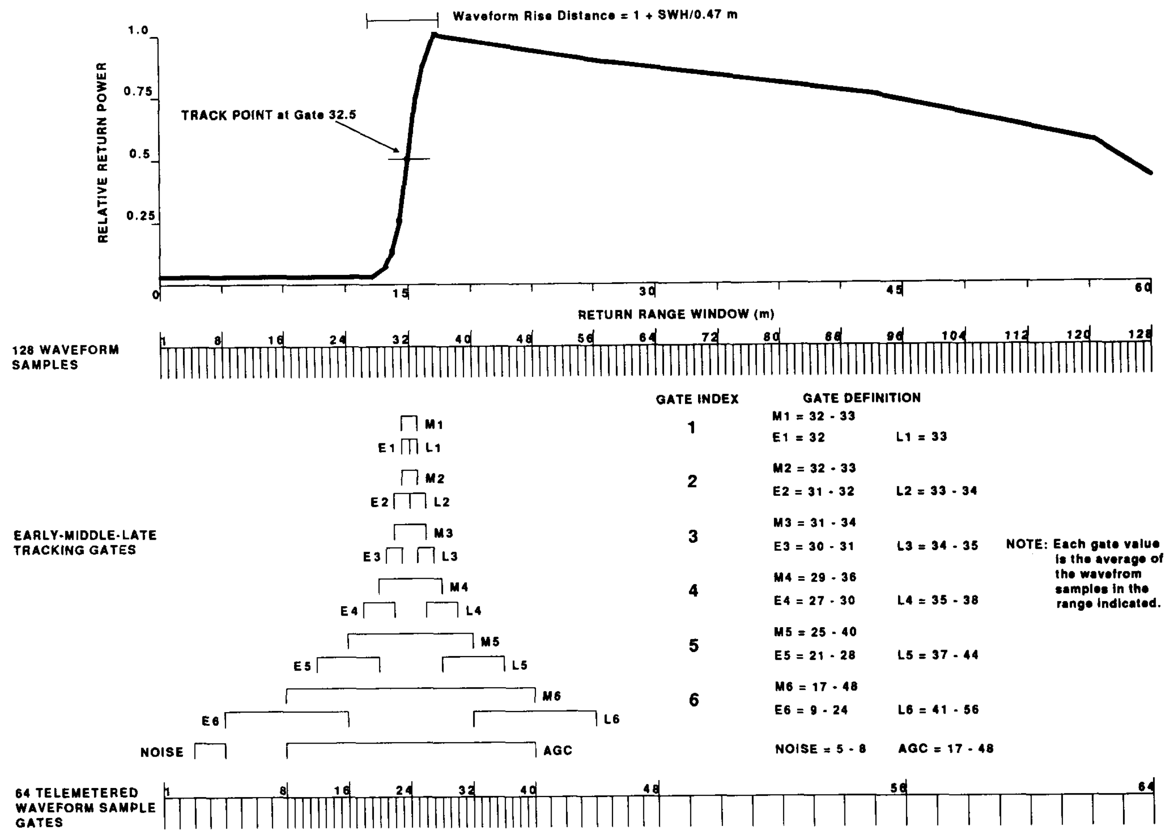

Fig. 6. Simplified waveform for the NASA TOPEX altimeter. Also shown are the noise, AGC, and middle gate definitions. The middle gate index is chosen based on the slope of the waveform, which itself depends on the SWH of the ocean.

The Middle gate is the average of 2, 4, 8, or 16 waveform samples, depending on the gate index used. There are five possible gate index values. As with the AGC gate, the noise gate value is subtracted from the initial Middle gate calculation. The waveform samples averaged for each gate index value are shown in Table II. The Early-Middle-Late tracker adjusts the altimeter height such that the Middle gate is equal to the AGC gate. A difference between these values is the error signal that is used as the input to the height tracker loop, which is discussed in detail below.

The Early and Late gates are used to select the gate index and to compute the significant wave height. The choice of the gate index is based on the significant wave height, which is inferred from the slope of the leading edge of the waveform. As the significant wave height increases, the gate index increases. This results in more waveform samples being used in the calculation of the height error, which helps to overcome the fact that the lower slope of the waveform edge makes the Middle gate value less sensitive to changes in the altimeter height.

The various gate definitions in Fig. 6 have evolved from the SEASAT and GEOSAT altimeter experience with tailoring to account for differences in the TOPEX ocean return such as the narrower antenna beamwidth at *Ku*-band and the addition of the *C*-band channel.

B. The Tracker Response

The TOPEX altimeter alpha-beta tracker is designed to filter out noise in the height estimates and to provide an estimate of the height rate that can be used in the pulse-to-pulse adjustment of the fine-height within the digital filter bank. The operation of the tracker can be represented by the following equations:

$$h_{n+2} = h_{n+1} + r_{n+1} + \alpha \Delta h_n \tag{1}$$

and

$$r_{n+2} = r_{n+1} + \beta \Delta h_n \tag{2}$$

where h_n is the tracker height, r_n is the tracker height rate, Δh_n is the measured height error for the nth tracker interval. The parameters α and β have values of $1/4$ and $1/64$ for the high resolution tracking mode. An alpha-beta tracker is used for both *Ku*- and *C*-band. The *C*-band tracking makes use of the *Ku*-band height rate, however.

The height error is the difference between the actual height and the tracker height. This is determined from the signal processor analysis of the middle and AGC gates. This error can be written as

$$\Delta h_n = \hat{h}_n - h_n \tag{3}$$

where $\hat{h}_n$ is the actual altimeter height.

TABLE III
Z-TRANSFORM COEFFICIENTS AND ROOTS FOR $\alpha - \beta$ TRACKER WITH $\alpha = 1/4$ AND $\beta = 1/64$

k	c_k	d_k	q_k
1	-0.086369	-0.015625	0.904509
2	0.562497	0.046875	0.75
3	-.226128	-0.015625	0.345492

By performing a z-transform analysis of this tracking loop, it can be shown that the tracker height and height rate can be related to the measured height by the following equations:

$$h_n = \sum_{k=1}^{3} c_k \sum_{l=0}^{\infty} q_k^l \hat{h}_{n-l-2} \tag{4}$$

and

$$r_n = \sum_{k=1}^{3} d_k \sum_{i=0}^{\infty} q_k^i \hat{h}_{n-i-2} \tag{5}$$

where the values of c_k, d_k, and q_k are given in Table III.

We can consider the case of the height being a quadratic function of time, represented as

$$\hat{h}_n = h_o + \nu n\tau + an^2\tau^2/2 \tag{6}$$

where τ is the length of the track interval (53 ms), ν is the rate of change of the height, and a is the height acceleration. In this case, the tracker output will be equal to

$$h_n = h_o + \nu n\tau + an^2\tau^2/2 + 64a\tau^2. \tag{7}$$

It can be seen here that the tracker correctly follows linear changes in the height, but makes an error due to constant acceleration. The maximum acceleration of interest is 1 $\mathrm{m/s^2}$. This will result in an uncorrected height error of 18 cm. This is an error that will be corrected in ground processing of the altimeter data.

We can also consider the response of the tracker to noise in the height measurement that is independent from one track interval to the next. Two sources of such noise are receiver noise and speckle noise. Using (4) we can find the variance of the tracker height in terms of the variance of the noise. The result is

$$\mathrm{var}\{h\} = \mathrm{var}\{\mathrm{noise}\} \sum_{k,k'=1}^{3} \frac{c_k c_{k'}}{1 - q_k q_{k'}} = \mathrm{var}\{\mathrm{noise}\} \times 0.234 \tag{8}$$

This equation follows from the previous definition of the tracker output. The tracker performs some filtering of noise that is independent from one track interval to the next, but it only removes about 75% of this noise power.

C. Instrument Noise Estimates

This section will address the impact of thermal receiver noise and ocean surface backscatter speckle noise on the height measurement, and demonstrate that the predicted noise performance satisfies the requirements for basin scale ocean topography. These noise sources are inherent in the instrument design and approach.

The single-pulse SNR can be determined from the standard radar equation

$$\frac{S}{N} = \frac{P_t G A \sigma \tau}{(4\pi)^2 k T N_F R^4} \tag{9}$$

where P_t is the transmitted power (20 W at *Ku*-band, 20 W at *C*-band), G is the antenna gain (46.6 dB at *Ku*-band, 38.4 dB at *C*-band), A is the antenna area (1.77 m^2), σ is the radar cross section of the illuminated surface, τ is the transmitted pule length (102.4 μs), k is Boltzmann's constant $(1.38 \times 10^{-23}\ \mathrm{J/K})$, T is the antenna temperature (300 K), N_F is the receiver noise figure (5 dB), and R is the altimeter height (1334 km).

The reflectivity of the ocean surface varies with the significant wave height of the ocean surface and with the wind speed. For illustration, we will use a value of 10 dB for the normalized radar cross section. The diameter of the illuminated area at low significant wave heights is about 2 km. Using these numbers results in a radar cross section of $3.1 \times 10^7\ \mathrm{m}^2$.

The SNR for one transmitted pulse is then found to be 29 dB for *Ku*-band and 21 dB for *C*-band. The SNR improved by the integration of several pulses. This noise will not limit the height measurement, however.

An even larger source of noise in the altimeter waveform is speckle noise, which was discussed above. The standard deviation of each measured waveform value is equal to its mean value. This is very much larger than the uncertainty introduced by the receiver noise. At this point, we can ignore the impact of receiver noise on the height measurement accuracy, and consider only the speckle noise limit.

The signal processor determines the height error by comparing the value of the Middle gate to the value of the AGC gate. Noise in these gate values will result in noise in the height error measurement. The number of waveform points in the middle gate is 2, 4, 8, or 16 depending on the significant wave height. Larger values are used for larger values of the waveheight. The number of waveform points used to compute the AGC gate is 32, independent of the gate index being used. These waveform points are themselves the average of 228 pulses for *Ku*-band and 60 pulses for *C*-band.

In order to estimate the impact of speckle noise on the final height measurement, we must make a few assumptions and approximations. First, we will represent the waveform shape as that of a Gaussian cumulative function given by the expression

$$F(h) = \frac{1}{\sqrt{2\pi}\sigma} \int_{-\infty}^{h} \exp\left(-\frac{x^2}{2\sigma^2}\right) dx. \tag{10}$$

The standard deviation of the Gaussian results from a convolution of the ocean surface height distribution and the compressed pulse shape. Following Brown [47], we write this standard deviation as

$$\sigma = \sqrt{(SWH/4)^2 + (0.425c\tau/2)^2} \tag{11}$$

where the factor of 0.425 comes from approximating the compressed pulse shape by a Gaussian function. The quantity $c\tau/2$ is the compressed pulse length.

To first order, the difference between the Middle gate and the AGC gate is a linear function of the height error. The proportionality can be found by using the above waveform approximation and changing the height by one-half of a filter-bin width and determining the corresponding change in the difference between the Middle gate and the AGC gates. We can then write the standard deviation of the height in terms of the standard deviation of the gate difference as

$$\mathrm{std}\{h\} = \frac{\mathrm{std}\{G_M - G_{AGC}\}}{S} \tag{12}$$

where G_M = Middle gate and G_{AGC} =AGC gate

$$S = \text{slope} = \frac{\Delta(G_M - G_{AGC})}{\Delta h}. \tag{13}$$

Since we have normalized the waveform plateau to have a value of 1 in the definition of $F(h)$ above, the standard deviation of a single waveform sample in the Middle gate is equal to its mean value of 0.5. This follows from the negative exponential distribution of these values determined from a single pulse. This standard deviation is reduced by averaging several waveform samples and by averaging several waveforms. The waveform samples are essentially independent of each other because they result from scattering from different areas of the ocean surface. The successive waveforms are not independent of each other because of the high repetition rate. This is described by Walsh [48]. We will then write

$$\mathrm{std}\{G_M - G_{AGC}\} = \frac{0.5}{\sqrt{M \times N_{\mathrm{eff}}}} \tag{14}$$

where M is the number of waveform samples used to compute the Middle gate (G_M), G_{AGC} is the AGC gate, and N_{eff} is the number of effectively independent pulses in a 3-s interval.

In order to correct for the free electron content of the atmosphere, the *Ku*- and *C*-band heights are combined to form a single, corrected height. The increase in the effective path length is inversely proportional to the square of the radar frequency. The corrected height is, therefore,

$$h_{\mathrm{comb}} = \frac{f_{Ku}^2 h_{Ku} - f_c^2 h_c}{f_{Ku}^2 - f_c^2} = 1.18 h_{Ku} - 0.18 h_c \tag{15}$$

and the standard deviation of the combined height can be computed as

$$\mathrm{std}\{h_{\mathrm{comb}}\} = \sqrt{(1.18x\ \mathrm{std}\{h_{Ku}\})^2 + (0.18x\ \mathrm{std}\{h_c\})^2}. \tag{16}$$

Combining the above results, we can compute the speckle limited height measurement uncertainty as shown in Table IV. These combined uncertainties are 1.24, 1.57, and 2.42 cm for significant wave heights of 2, 4, and 8 m. The system requirements are 1.7, 2.1, and 3.0 cm, as stated earlier. The final system precision results from several factors:

- The transmit power and the antenna gain are sufficient to make receiver noise a minor part of the measurement uncertainty; speckle noise will dominate.
- Increasing the Middle gate width as the significant wave height increases compensates for the decreased slope of the waveform.
- The high pulse repetition rate results in the maximum number of independent pulses being available to the tracker. The effective number of independent pulses is not limited by the pulse repetition rate.

TABLE IV
MEASUREMENT UNCERTAINTY DUE TO SPECKLE NOISE LIMITS FOR 3-S AVERAGES OF THE *Ku*-BAND, *C*-BAND, AND COMBINED HEIGHT

SWH	σ (m)	M*	Slope (m^{-1})	Neff		Height Std Dev (cm)		
				Ku	C	Ku	C	Comb
2	0.538	2	0.2677	3641	1405	1.03	1.65	1.24
4	1.020	4	0.1280	4966	1917	1.30	2.09	1.57
8	2.010	8	0.0497	6953	2684	2.00	3.21	2.42

*M = Middle Gate width (i.e., number of waveform samples used)

The values shown in Table IV represent only the limits imposed on the height measurement by the speckle noise. System calibration and ground testing are required in order to establish the fact that these values are approached by the complete, functioning altimeter system.

D. Calibration Modes

The TOPEX altimeter design includes two calibration modes. When commanded to enter calibration mode, the altimeter enters Cal-I mode then proceeds to Cal-II.

In Cal-I mode, the altimeter is set up for simultaneous transmission and reception. A portion of the transmitter output is fed to the receiver through a digitally controlled attenuator and delay line. (Transmission and reception by the antenna is blocked in this mode by front-end switching.) Because the pulses are not reflected off the ocean, there is no spreading of the received signal and the input to the digital filter bank consists of a single frequency component (i.e., a point target).

The tracker adjusts the fine height to center the received point target signal between two waveform sample gates and the received AGC is set to produce a preset level at the receiver output. The attenuator is adjusted every 10 s in 2 dB steps through 17 preset values. By maintaining a history of the fine height and AGC settings during this process, changes in altimeter internal delay and gain are monitored. Delay changes are determined to a 7 mm accuracy and AGC to 0.25 dB.

Cal-I mode tracks changes in the altimeter's internal delay but does not measure its absolute value. This is accomplished during ground testing by use of a special hardware setup and subset of the Cal-I mode referred to as the height-bias test. A reflection point is established at a known distance from the phase center of the antenna feed. Transmitted pulses are reflected from this point and processed by the filter bank at a fixed AGC while the fine height is incremented over its full range. Analysis of the waveform sample data yields a measure of the altimeter's internal delay (i.e., relative delay between the transmit and receive paths of the altimeter). Changes in this delay are then tracked by the Cal-I mode during in-flight operation. The initial delay was measured to an accuracy less than 2 cm using the above technique.

Cal-II mode starts upon completion of Cal-I. In this mode the altimeter processes receiver thermal noise to provide a measure of the overall response of the receiver and filter bank combination. This allows compensation of the waveform sample data for artifacts of the altimeter processing. The AGC is adjusted to set the noise level at a predetermined value and the fine height is swept in this mode to account for the effects of the associated frequency shift. The resulting AGC is used to determine the initial setting during ocean return acquisition. The Cal-II mode runs until the altimeter is commanded to Standby in preparation for tracking.

Several other modes of operation are built into the TOPEX altimeter, but will not be discussed in detail here. These include scanning the full height interval for interference sources, a transmit test mode, and several system test modes. The occasional use of these modes, along with the continual monitoring of temperatures, voltages, currents, powers, and software memory ensure that the altimeter is operating as designed and that sufficient information is available to calibrate the resulting height measurements.

E. Surface Acquisition Timing

The TOPEX altimeter is designed to meet a requirement for the acquisition of surface tracking within 5 s of the transition from flight over land to flight over water. Acquisition is the process of the altimeter going from no knowledge of the altimeter height (except to place it within a window of 1274 to 1394 km) to tracking of the height at full resolution.

Acquisition begins by searching the full window from 1274 to 1394 km with 5 MHz bandwidth pulses. These pulses result in a resolution of 30 m. Each of the 128 digital filter bank samples of the waveforms corresponds to a distance of 3840 m. For the first track interval, pulses are transmitted and received for a height of 1274 km. The height is increased by 3240 m, then another track interval is processed. This continues until 39 track intervals have been processed. Pulses are transmitted for a 40th track interval, but the results are ultimately ignored. The waveforms for the 39 track intervals are searched to find the one waveform with the greatest magnitude of response. The position of this maximum response is also determined within the 3840 m filter bank extent. This represents the first step in the height determination. Transmitting pulses for 40 track intervals requires 2.12 s.

Acquisition proceeds by continuing to transmit pulses with a 5 MHz bandwidth for at least 20 track intervals. During this time, the tracking loop operates to refine the height estimate. If the waveform quality is judged to be sufficiently good, the altimeter will transition to high resolution tracking. The waveform quality assessment is based on the rms error in the height measurement over the last 10 track intervals and on the width of the waveform. Unlike the broad waveforms observed with full bandwidth pulses, the low bandwidth pulses result in narrow, sharply peaked waveforms.

If at the end of 20 track intervals, the waveform quality is judged not good enough to begin high resolution tracking, the altimeter may begin high resolution acquisition, drop all the way back to low resolution acquisition, or continue low resolution tracking for 10 more track intervals. Each option depends on the quality of the waveforms and the height statistics, with the poorest quality waveforms resulting in beginning again at low resolution acquisition. Low resolution tracking always takes at least 1.06 sec. The decision to transition to another mode is made at that time, or at 0.53-s intervals thereafter.

The minimum time required to begin high-resolution tracking is therefore 3.18 s. During low resolution tracking, only the coarse height is adjusted and this is done in 15-m steps. This coarse height applies to both altimeter channels. High resolution tracking therefore begins with only a rough estimate of the height. The signal processor will typically take on the order of 10 track intervals to settle the height and height rate estimates. From that point on, the waveforms that result from the digital filter bank differ very little from one track interval to the next, and long-term statistical assessments are required to establish the height precision. This settling occurs in about 1 s.

The acquisition process is therefore seen to require at least 3 s to transition to high resolution tracking and perhaps another second to settle the tracking loops. The performance requirement placed on the altimeter is acquisition within 5 s. Ground testing of the actual acquisition performance will be discussed later in this paper.

On a continuing basis, the signal processor reevaluates the quality of the waveforms and the rms variations in the height measurements. If these are found to be insufficient to continue high-resolution tracking, then one of the other modes will be commenced. These are, in order of increasing severity, high resolution acquisition, low resolution tracking, and low resolution acquisition. The signal processor will attempt to minimize the time spent in modes other than high resolution tracking by making the minimum change in operating mode necessary to reestablish high-quality tracking.

F. Radar Altimeter System Evaluator

The principle means of testing the TOPEX altimeter is the Radar Altimeter System Evaluator, or RASE. The RASE includes all of the systems necessary to send commands to the altimeter, record telemetry data from the altimeter, and generate simulated ocean backscatter. This last function is served by the Return Signal Simulator (RSS).

The RSS simulates the radar backscatter of the altimeter pulse from the ocean surface. This includes the following effects:

- Radar cross section of the ocean surface
- Significant wave height
- Satellite attitude angle
- Height, height rate, and height acceleration
- Speckle statistics of ocean backscatter
- Spatial and temporal correlation of speckle
- Dual-frequency altimeter operation
- Both 5 MHz (acquisition) and 320 MHz (tracking) pulse bandwidths

The RSS detects the pulse transmitted from the altimeter, determines the pulse frequency and bandwidth, calculates the round-trip delay time for the pulse based on the current height, then simulates and transmits the return pulse at the proper time.

The RSS creates the returned pulses by performing the following steps: A uniformly random distribution sequence is simulated using mutually prime shift registers, each generating an irreducible polynomial sequence. The outputs of the shift registers are mixed using exclusive-or gates. The uniform distribution is converted to a truncated Rayleigh distribution using a look-up table in read-only memory. Waveform amplitude points are multiplied by the Rayleigh coefficients to generate a waveform amplitude sequence with Rayleigh or speckle noise. A uniform random phase distribution sequence is generated by addressing a sine/cosine read-only memory with a uniform random sequence. The complex waveform is generated by multiplying the Rayleigh amplitude waveform by the uniform phase. Next, to simulate waveform correlation, a running average of each in-phase and quadrature-phase point is kept with the averaging coefficient proportional to the correlation for that point on the waveform. The complex waveform points are the inputs to the inverse Fast Fourier transform (FFT). After the inverse FFT, frequency shifting is performed by multiplying the output by a rotating phaser which has a rate proportional to the required frequency shift.

This process produces 128 complex values that include all of the proper statistics for the ocean surface reflection. These values are converted from digital to analog signals at a 1.25 MHz rate and used to modulate a 500 MHz carrier. This signal is then mixed with a locally generated pulse with a 320 MHz wide linear FM chirp and a center frequency of 13.1 GHz.

The last three steps of this process (Fourier transform, digital-to-analog conversion and modulation of a 500 MHz carrier, and mixing with a locally generated chirp pulse) are the reverse of the processing that takes place within the altimeter. The signal processor removes the chirp and mixes the received pulse to IF, mixes again to baseband and samples the result, then Fourier transforms the result and takes the square magnitude to produce the final waveforms.

The first step in the RSS process above accounts for the random amplitude and phase that results from backscatter from a large area of the ocean in which many independent phase facets contribute coherently to the total backscattered field. The mean values of these random numbers represent the ideal waveform that would result from the given significant wave height, surface radar cross section, and satellite attitude. The waveform will differ depending on the pulse bandwidth that is being transmitted.

The round-trip propagation time for the pulses is longer than the interpulse interval. For a given received pulse, the RSS will receive 37 more pulses at *Ku*-band before the reflected pulse is transmitted back to the altimeter.

Normal testing of the altimeter involves exercising all of the modes of operation of the altimeter with a wide variety of programmed conditions. In determining the height measurement performance, the altimeter is commanded to begin tracking, at which time it begins transmitting pulses with a 5 MHz bandwidth to determine the rough height of the altimeter. This is done by transmitting for one track interval at each height from 1274 to 1394 km, in steps of 3240 m. The RSS responds to each of these pulses with a delay that corresponds to the programmed height. After determining the coarse height, the altimeter will refine the height estimate by tracking the surface at the 5 MHz bandwidth. When certain track quality conditions are met, the altimeter will switch to high-resolution mode and begin transmitting 320 MHz bandwidth pulses. The RSS must recognize this change and respond accordingly.

The altimeter then proceeds to track at full bandwidth for many minutes. During this time, all of the science and engineering data in the telemetry channel are recorded. The science data include the tracker height, the height rate, the gate values and indices, and several other quantities for each track interval. The waveforms are also included in the telemetry, but after some averaging has taken place. The waveforms from two successive track intervals are averaged together in the telemetry. Further, the number of waveform samples is reduced from 128 to 64 by averaging groups of samples together. The first 16 samples are averaged in pairs, the next 32 are left unaveraged, the next 16 are again averaged in pairs, and the last 64 are averaged in groups of 4.

The telemetry data are used to generate statistics of the altimeter performance. The particular data products are discussed below. The design of the RSS allows for a realistic test of the altimeter functions and should represent an accurate picture of on-orbit performance of the TOPEX altimeter.

III. NASA TOPEX Altimeter Test Program

The altimeter has been subjected to a rigorous test program at the unit, system, and spacecraft levels for the purposes of quality assurance and performance assessment.

All units underwent vibration (3-axis sine and random) and thermal vacuum environmental tests. In many cases thermal tests were conducted prior to vibration and thermal vacuum to identify and correct problems before committing to more extensive tests. EMI/EMC tests were performed on units that interface with the spacecraft power bus or are significant RF sources. These are the travelling wave tube amplifier (TWTA), *C*-band solid state amplifier (CSSA), low voltage power supply (LVPS), and the up-converter frequency multiplier (UCFM). At the system or altimeter level, thermal vacuum and EMI/EMC tests were conducted. Due to the configuration of the altimeter, vibration or acoustic tests were not feasible.

Since integration with the spacecraft, EMI/EMC, vibration (single-axis sine), acoustic, and thermal vacuum tests have been accomplished. With the exception of the TWTA, the altimeter was powered in a *C*-band-only calibration mode during the vibration and acoustic tests. (The TWTA is at risk if it is subjected to such tests with a hot cathode.) In addition, the altimeter has been an active participant during spacecraft tests with the Project Operations Control Center (POCC at JPL) and the communications network.

Before, during, and after each of the major environmental tests at the unit, system and spacecraft levels, performance testing has been conducted plus various calibration tests were performed. Table V summarizes the environmental test program.

TABLE V
SUMMARY OF THE NASA TOPEX ALTIMETER ENVIRONMENTAL TEST PROGRAM

Test	Unit	System	Spacecraft
EMI/EMC	Selected Units	Y	Y (including ESD)
Thermal	Y	N	N
Vibration	Sine & Random	N	Sine
Acoustic	N	N	Y
Thermal Vacuum	6 Cycles	5 Cycles	30 Days
Pyro Shock	N	N	Y

TABLE VI
RANGE OF SIGNAL PARAMETERS EMPLOYED DURING TESTING

Range of Signal Parameters Employed During Testing	
Height (km)	1274, 1334, 1394
Height Rate (m/s)	0, +/-25, +/-50
Height Acceleration (m/s^2)	0, +/-1.0
Ku/C Height Differential (cm)	100, 130, 160
Backscatter Coefficient (dB)	3 to 20
Off-Nadir Angle (deg)	0, 0.24, 0.35, 0.42
SWH (Significant Wave Height) (m)	0.63, 1.64, 4.14, 5.6, 8.44, 12.7, 19.9

TABLE VII
ACQUISITION PERFORMANCE (MEDIUM TIME IN SECONDS FOR SEARCH, ACQUISITION AND SETTLING—SEA STATE RANGE = 2 TO 8 m, *C*-BAND CHANNEL BANDWIDTH = 320 MHz)

	Side A (sec)	Side B (sec)
Ku	6.4	6.4
C	6.9	6.6
Ku/C Combined	6.7	6.5

TABLE VIII
SIGNIFICANT WAVE HEIGHT MEASUREMENT PERFORMANCE.

	SWH (m)	Spec (m)	Mean Error (m)		Error Std-Dev (m)	
			Side A	Side B	Side A	Side B
Ku	2	+/-0.5	-0.05	0.14	0.03	0.10
	4	+/-0.5	-0.12	0.16	0.04	0.17
	8	+/-0.8	-0.16	0.15	0.07	0.26
C	2	+/-0.5	0.02	0.35	0.04	0.03
	4	+/-0.5	-0.06	0.32	0.07	0.06
	8	+/-0.8	-0.06	0.36	0.14	0.10

A. Performance Test Results—Track Mode

An automated series of performance test sequences was used to assess the altimeter's acquisition and tracking characteristics throughout the test program at the system and spacecraft levels of integration. For the majority of tests, two-altimeter, dual-channel tracking configurations were employed: *Ku* channel primary with the secondary *C*-band channel set for full bandwidth operation (i.e., 320 MHz) and *Ku* channel primary with the secondary *C*-band channel operating in the reduced bandwidth option (i.e., 100 MHz). Other possible altimeter configurations such as single channel operation, (*Ku*- or *C*-band) and dual channel operation with *C*-band primary and *Ku* secondary were tested early-on but were dropped later to confine testing to a reasonable time duration.

The test sequences vary the configuration of the simulated ocean return signal with respect to: significant wave height (SWH), off-nadir angle (ONA), initial height, height rate, height acceleration, height difference between the *Ku*- and *C*-channels and *Ku*- and *C*-return signal strengths (sigma-zero). The various return signal parameters used throughout the altimeter test program are presented in Table VI.

For each simulated return signal configuration, a 3-minute run of tracking data was obtained starting with signal acquisition. This process was initiated by commanding the altimeter from Stand-by to the Track mode. Each track run or trial was analyzed to determine the altimeter's characteristics regarding:

- Acquisition
- SWH determination
- Height tracking
- Ocean backscatter coefficient (sigma-zero) resolution
- Ionospheric effects (i.e., *Ku/C* height difference)

Acquisition Results: The altimeter has a requirement to achieve ocean return signal tracking at specified quality levels within 5 s of initiation of acquisition with regard to height tracking, height rate estimation, SWH determination, and AGC settling. This requirement is dictated by the desire to obtain quality data as soon as possible when the satellite's sub-track transitions from land to sea. Table VII presents a representative summary of the altimeter's measured acquisition performance. While the results are somewhat greater than specified, there are several mitigating factors that bode well for performance in orbit.

First, the testing required a search for the ocean return over a 120 km height extent to demonstrate operation over the range of possible TOPEX altitudes. The height variation of the actual TOPEX orbit will be much less, on the order to 30 km. Adjusting the search via uploaded parameters to that actually needed will reduce the search time proportionately. The reduction from 120 to 30 km reduces the search time by one-fourth to 0.5 s.

Second, the altimeter tracking algorithms are adaptive and, in most cases, expected to be tracking land return using the coarse resolution mode when crossing the land-to-sea boundary. This eliminates a search for the return signal and allows for rapid settling of the ocean return tracking.

Third, the equipment producing the simulated ocean return, the RSS, must itself acquire and synchronize with the altimeter's transmitted signal. This uses additional time that affects the altimeter's acquisition that will not be present with the actual ocean return.

SWH Determination: The altimeter is designed to provide an estimate of SWH to an accuracy of 0.5 m or 10% of SWH, whichever is greater. The data from each track scenario were examined for compliance with this requirement. The altimeter SWH data were corrected to remove a bias caused by any mismatch of the chirp signals of the altimeter's transmission and RSS return. This mismatch will not be present with the ocean reflections. Table VIII shows typical test results which are well within the stated requirements.

Height Tracking: To assess tracking performance, the height data for each trial are averaged over intervals of 1 and 3 s. Curves, linear, or higher order as appropriate, are fitted to the 1 and 3 s averaged data and the standard deviation of the fit

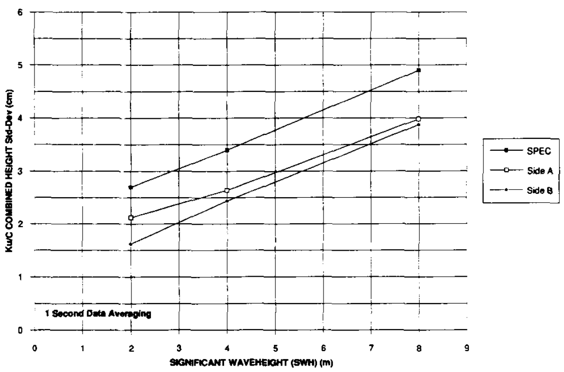

Fig. 7. *Ku*/*C*-band (320 MHz bandwidth) combined height standard deviation vs SWH-1-s averaging.

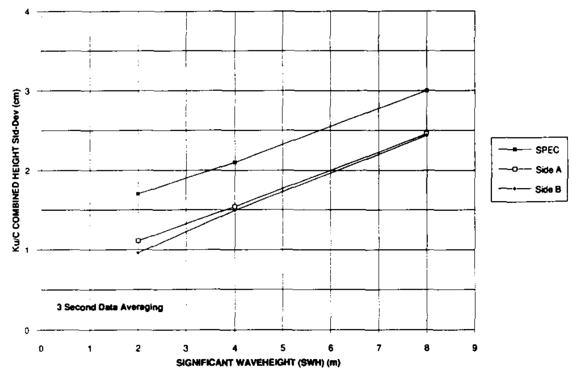

Fig. 8. *Ku*/*C*-band (320 MHz bandwidth) combined height standard deviation vs SWH-3-s averaging.

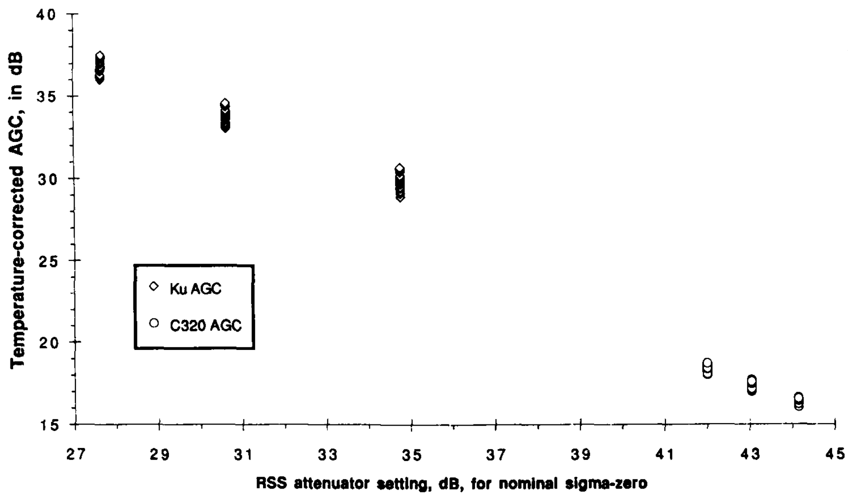

Fig. 9. *Ku*- and *C*-band temperature corrected AGC values versus RSS attenuator setting.

residuals computed. The standard deviations are compared to specified values for the tracking assessment.

Tracking performance for 2, 4, and 8 m SWH have been specified for both single channel and combined, dual-channel operation. Figs. 7 and 8 present combined height results for 1 and 3 s averaging at each of the three specified significant wave heights for the dual channel configuration. These results are "aggregate" standard deviations derived from a large body of track trials. In all cases the altimeter's performance is comfortably within specifications.

Ocean Backscatter Coefficient (Sigma-Zero) Resolution: The altimeter is required to resolve the ocean backscatter coefficient to an accuracy of $+/-1$ dB with a precision of $+/-0.25$ dB. The test sequences provide return signals at nominal, high and low sigma-zero conditions for each SWH. The nominal values are from [50]. The high and low values are typically $+/-6$ dB from the nominal valve.

Fig. 9 shows the results of test cases used for nominal values used for testing related to 2, 4, and 8 m SWH. The data are for all performance level tests performed with the nominal sigma zero since the integrated satellite was delivered to GSFC for final testing. The relationship of the AGC to sigma zero can be seen in the plots. Also, the repeatability of the AGC can be seen by the scatter of the data. Except for one point, the *Ku*-band AGC values are all within 1 dB of the mean value in each group. The *C*-band values are within 0.5 dB of the mean value. This scatter also includes any variations in the RASE setup, though this contribution has not been quantified.

Ionospheric Effects: The altimeter has a requirement to measure the height differential between the *Ku*- and *C*-band channels produced by a total electron count of 200 TECU with a resolution of $+/-4$ TECU. (TECU stands for total electron count unit; one TECU is $4 \times 10^{+16}$ free electrons per square meter.)

The height differential between the *Ku*- and *C*-band channels corresponding to 200 TECU is approximately 2.4 m. The altimeter has a total height differential capability of 2.8 m, which was verified during altimeter integration. For routine testing, the maximum height differential range is limited by the test equipment to about 30 cm.

Fig. 10 is a plot of the height difference for tests performed during the spacecraft thermal vacuum test for a SWH of 2, 4, and 8 m.

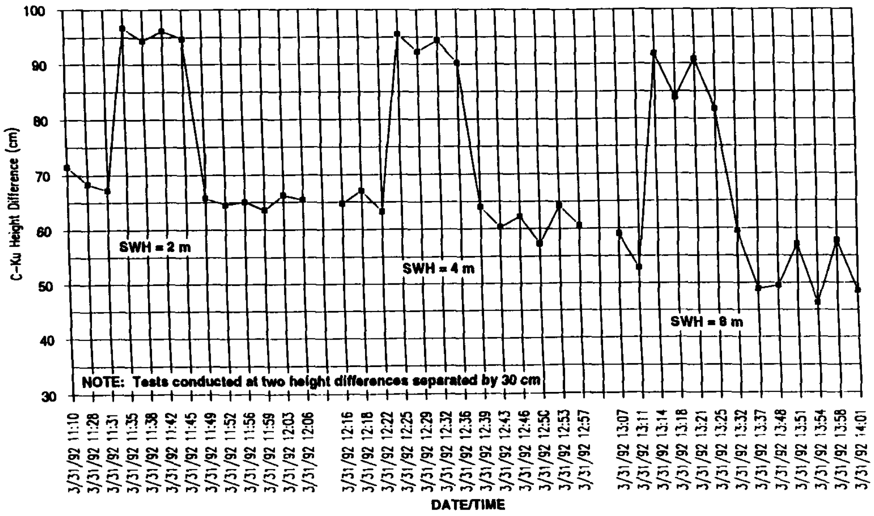

Fig. 10. *C-Ku*-band height difference at 2, 4, and 8 m SWH.

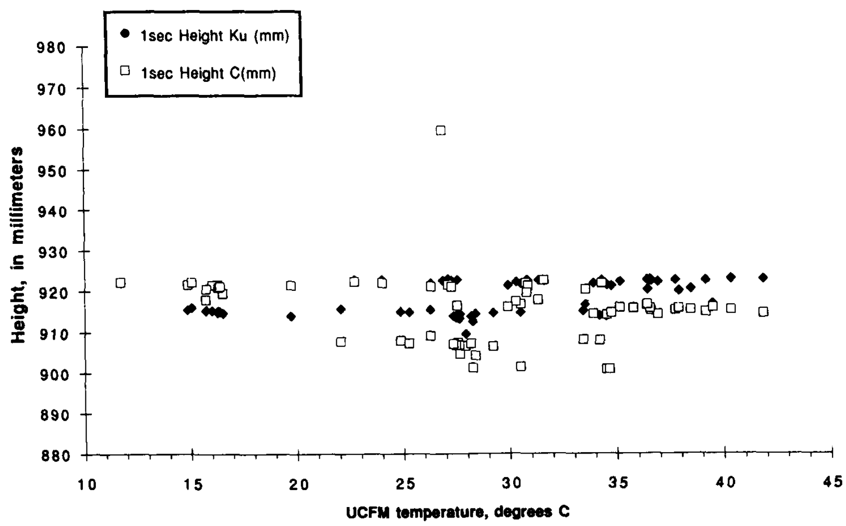

Fig. 11. Altimeter height versus UCFM temperature. The height is seen to have only a weak dependence on the temperature. No correction for temperature is required.

B. Performance Test Results—Calibrate Mode

During the spacecraft thermal vacuum test, the altimeter was operated in the calibrate mode which consists of 17 signal levels (Cal-I). Step 6 of the Cal-I is used to show the repeatability of the height measurement, which provides a relative measure of the change in altimeter internal delay. By monitoring these measurements since the initial determination of the altimeter internal delay (refer to Section D), any delay drift can be determined and appropriate adjustment made to the altimeter height data. Fig. 11 shows the height from all Cal-I runs since satellite delivery to GSFC and before shipment to the launch site. (Note that changes in the height of Fig. 11 are of concern and not the absolute height reading.) These data span 5 months and temperatures from 10 to 35°C. The Cal-I mode design has a 7 mm height resolution limitation, which can be seen in the data. The calibration mode meets its specification for the ability to detect height changes greater than 1.5 cm. These data indicate that there is no height correction required related to temperature. The TOPEX system in flight is expected to operate between 20 and 30°C. Since the orbital temperature excursions will be much more restricted in orbit than experienced during the thermal vacuum test, it can be expected that the height bias changes due to temperature will be well below 1 cm.

From the same data set, the AGC is shown in Fig. 12 with no temperature correction. The requirement for a temperature

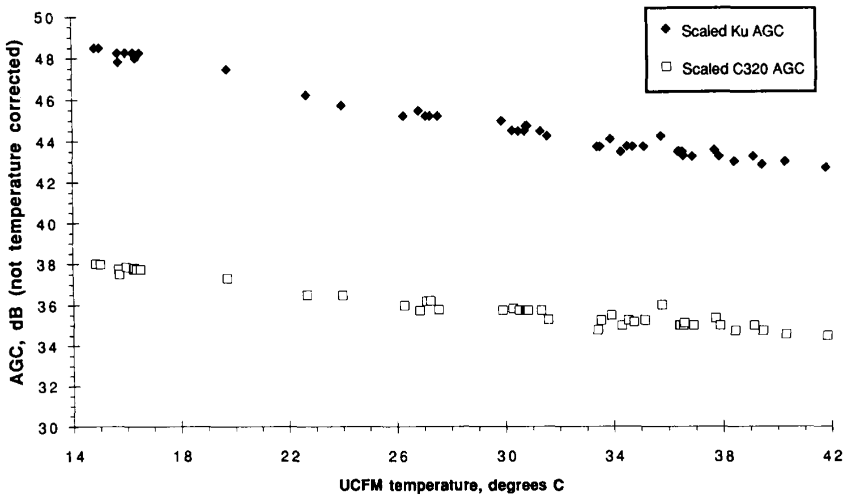

Fig. 12. Altimeter AGC versus UCFM temperature. The AGC is seen to have a significant dependence on the temperature, requiring a correction in the ground processing of the data.

correction of AGC is obvious. Over the range from 20 to 30°C, the *Ku*-band AGC changes by 3 dB. The data can be corrected for temperature, and it can be seen that the repeatability satisfies the specification (to detect changes greater than 0.25 dB).

IV. Conclusion

Theoretical analysis predicted and prelaunch testing demonstrated the capability of the TOPEX altimeter to measure the range to the ocean surface with 2 cm range and accuracy. Given continued success, the measurement of basin-scale ocean circulation will soon be an accomplished fact.

References

[1] C. J. Koblinsky, P. Gaspar, and G. Lagerloef, Eds., "The future of spaceborne altimetry: Oceans and climate change," *Joint Oceanographic Institutions Inc.*, Washington, DC.

[2] K. A. Kelly and S. T. Gille, "Gulf stream surface transport and statistics at 69°W from the GEOSAT altimeter," *J. Geophys. Res.*, vol. 95, pp. 3149–3161, 1990.

[3] J. Vazquez, V. Zlotnicki, and L. L. Fu, "Sea level variabilities in the gulf stream between Cape Hatteras and 50°W: A GEOSAT study," *J. Geophys. Res.*, vol. 95, pp. 17957–19764, 1990.

[4] B. D. Tapley, R. S. Nerem, C. K. Shum, J. C. Ries, and D. N. Yuan, "Determination of the general ocean circulation from the joint gravity field solution," *Geophys. Res. Lett.*, vol. 15, pp. 1109–1112, 1988.

[5] J. G. Marsh, C. J. Koblinsky, F. J. Lerch, S. M. Klosko, J. W. Robbins, R. G. Williamson, and G. B. Patel, "Dynamic sea surface topography, gravity, and improved orbit accuracies from the direct evaluation of SEASAT altimeter data," *J. Geophys. Res.*, vol. 95, pp. 13129–13150, 1990.

[6] R. S. Nerem, B. D. Tapley, and C. K. Shum, "Determination of the ocean circulation using GEOSAT altimetry," *J. Geophys. Res.*, vol. 95, pp. 3163–3179, 1990.

[7] R. S. Nerem, C. J. Koblinsky, R. G. Williamson, and S. M. Klosko, "Observing large-scale sea surface topography from space; Part I—Techniques and initial results," *J. Geophys. Res.*, submitted, 1992.

[8] L. Miller, R. E. Cheney, and B. C. Douglas, "GEOSAT altimeter observations of Kelvin waves and the 1986-87 El Nino," *Science*, vol. 239, pp. 52–54, 1988.

[9] D. B. Chelton, M. G. Schlax, D. L. Witter, and J. G. Richman, "GEOSAT altimeter observations of the surface circulation of the Southern Ocean," *J. Geophys. Res.*, vol. 95, pp. 17877–17903, 1990.

[10] C. Wunsch, "Global-scale sea surface topography from combined altimetric and tide gauge measurements," *J. Geophys. Res.*, vol. 96, pp. 15053–15082, 1991.

[11] R. E. Cheney, J. G. Marsh, and B. D. Beckley, "Global mesoscale variability from colinear tracks of SEASAT altimeter data," *J Geophys. Res.*, vol. 88, pp. 4343–4354, 1983.

[12] D. T. Sandwell, and B. Zhang, "Global mesoscale variability from the GEOSAT Exact Repeat Mission—Correlation with ocean depth," *J Geophys. Res.*, vol. 94, pp. 17971–17984, 1989.

[13] V. Zlotnicki, L.-L. Fu, and W. Patzert, "Seasonal variability in global sea level observed with GEOSAT altimetry," *J Geophys. Res.*, vol. 94, pp. 17959–17969, 1989.

[14] P. Y. LeTraon, M. C. Rouquet, and C. Boissier, "Spatial scales of mesoscale variability in the North Atlantic as deduced from GEOSAT data," *J Geophys. Res.*, vol. 95, pp. 20267–20285, 1990.

[15] P. T. Le Traon, "Time scales of mesoscale variability and their relationship with space scales in the North Atlantic," *J. Marine Res.*, vol. 49, pp. 1–26, 1991.

[16] P. DeMay and Y. Menard, "Synoptic analysis and dynamical adjustment of GEOS-3 and SEASAT altimeter eddy fields in the northwest Atlantic," *J. Geophys. Res.*, vol. 94, pp. 6221–6230, 1989.

[17] V. Zlotnicki, "Sea level differences across the Gulf Stream and Kuroshio Extension," *J. Geophys. Res.*, vol. 21, pp. 599–609, 1991.

[18] C. W. Horton, D. L. Porter, P. W. DeWitt, and W. E. Rankin, "Airborne expendable bathythermograph survey of the Kuroshio extension and comparison with simultaneous altimeter measurements during the GEOSAT exact repeat mission," *J. Geophys. Res.*, vol. 97, pp. 7447–7463, 1992.

[19] P. DeMay and A. R. Robinson, "Assimilation of altimeter eddy fields in a limited area quasi-geostrophic model," *J. Geophys. Oceanog.*, vol. 17, pp. 2281–2293, 1987.

[20] A. R. Robinson and L. J. Walsted, "Altimetric data assimilation for ocean dynamics and forecasting," *JHU/APL Tech. Digest*, vol. 8, pp. 267–271, 1987.

[21] P. Malanotte-Rizzoli and W. R. Holland, "Assimilation of altimeter data into an ocean circulation model: Space versus time resolution studies," *J. Phys. Oceanog.*, vol. 19, pp. 1507–1534, 1989.

[22] J. Verron, "Altimeter data assimilation into an ocean circulation model: sensitivity to orbital parameters," *J. Geophys. Res.*, vol. 95, pp. 11443–11459, 1990.

[23] J. Verron, "Nudging satellite altimeter data into quasigeostrophic ocean models, *J. Geophys. Res.*, submitted, 1992.

[24] B. J. Haines, G. H. Born, G. W. Rosborough, J. G. Marsh, and R. G. Williamson, "Precise orbit computation for GEOSAT Exact Repeat Mission," *J. Geophys. Res.*, vol. 95, pp. 2871–2886, 1991.

[25] The Navy GEOSAT Mission, *JHU/APL Tech. Digest*, vol. 8, no. 2, Apr. 1987.

[26] APL Ocean Sciences, *JHU/APL Tech. Digest*, vol. 10, no. 4, Oct. 1989.

[27] GEOS 3 Special Issue, *J. Geophys. Res.*, vol. 84, no. B8, pp. 3779–3079, July 1979.
[28] SEASAT Special Issue I: Geophysical Evaluation, *J. Geophys. Res.*, vol. 87, no. C5, pp. 3173–3438, Apr. 1982.
[29] SEASAT Special Issue II: Scientific Results, *J. Geophys. Res.*, vol. 88, no. C3, pp. 1529–1952, Feb. 1983.
[30] GEOSAT Special Issue Part I, *J. Geophys. Res.*, vol. 95, no. C3, Mar. 1990.
[31] GEOSAT Special Issue Part 2, *J. Geophys. Res.*, Vol. 95, no. C10, Oct. 1990.
[32] D. L. Porter, E. B. Dobson, and S. M. Glen, "Measurements of Dynamic topography during SYNOP Utilizing a GEOSAT Synthetic Geoid," *Geophys. Res. Lett.*, submitted, 1992.
[33] S. M. Glenn, D. L. Porter, and A. R. Robinson, "Synthetic geoid validation of GEOSAT mesoscale dynamic topography in the gulf stream region," *J. Geophys. Res.*, vol. 96, pp. 7145–7166, 1991.
[34] D. L. Porter, A. R. Robinson, S. M. Glenn, and E. B. Dobson, "The synthetic geoid and the estimation of mesoscale absolute topography from altimeter data," *JHU/APL Tech. Digest.*, vol. 10, No. 4, pp. 369–379, 1989.
[35] J. L. Mitchell, J. M. Dastugue, W. J. Teague, and Z. R. Hallock, "The estimation of geoid profiles in the northwest Atlantic from simultaneous satellite altimetry and airborne expendable bathythermograph sections," *J. Geophys. Res.*, vol. 95, pp. 17965–17977, 1990.
[36] M. R. Carnes, J. L. Mitchell, and P. W. deWitt, "Synthetic temperature profiles derived from GEOSAT altimetry: Comparison with air-dropped expendable bathythermograph profiles," *J. Geophys. Res.*, vol. 95, pp. 17979–17992, 1990.
[37] K. A. Kelly, A. and D. R. Watts, "Comparison of surface and baroclinic transport fluctuations in the gulf stream at 68°W," *EOS, Transactions, American Geophysical Union*, vol. 72, no. 51, p. 57, Dec. 1991.
[38] Satellite Altimetric Measurements of the Ocean: Report of the TOPEX Science Working Group, *NASA*, JPL, Caltech, 1981.
[39] F. Monaldo, "TOPEX ionospheric height correction precision estimated from prelaunch test results," *IEEE Trans. Geosci. Remote Sensing*, submitted 1992.
[40] R. S. Nerem, B. H. Putney, J. A. Marshall, F. J. Lerch, E. C. Pavlis, S. M. Klosko, S. B. Luthcke, R. G. Williamson, and N. P. Zelensky, "Expected orbit determination performance for the TOPEX/POSEIDON mission," *IEEE Trans. Geosci. Remote Sensing*, submitted 1992.
[41] E. J. Walsh, D. Vandemark, D. E. Hines, L. G. Hevizi, R. E. McIntosh, R. N. Swift, and J. F. Scott, "Electromagnetic bias in the sea surface range measurements of the TOPEX/POSEIDON satellite," *IEEE Trans. Geosci. Remote Sensing*, submitted 1992.
[42] R. D. Ray, "Global ocean tide models on the eve of TOPEX," *IEEE Trans. Geosci. Remote Sensing*, submitted 1992.
[43] R. H. Rapp, "Geoid undulation accuracy for the TOPEX/POSEIDON Mission, *IEEE Trans. Geosci. Remote Sensing*, submitted 1992.
[44] D. B. Chelton, E. J. Walsh, and J. L. MacArthur, "Pulse compression and sea level tracking in satellite altimetry," *J. Geophys. Res.*, vol. 6, no. 3, pp. 407–438, June, 1989.
[45] J. L. MacArthur, C. C. Kilgus, C. A. Twigg, and P. V. K. Brown, "Evolution of the satellite radar altimeter," *JHU/APL Tech. Digest.*, vol. 10, no. 4, pp. 405–413, Oct. 1989.
[46] A. R. Zieger, D. W. Hancock, G. S. Hayne, and C. L. Purdy, "NASA radar altimeter for the TOPEX/POSEIDON project," *IEEE Proc.*, vol. 79, no. 6, June 1991.
[47] G. S. Brown, "The average impulse response of a rough surface and its applications," *IEEE Trans. Antennas Propagat.*, vol. 25, pp. 67–74, 1977.
[48] E. J. Walsh, "Pulse-to-pulse correlation in satellite radar altimeters," *Radio Sci.*, vol. 17, pp. 786–800, 1982.
[49] "Requirements and constraints for the NASA Radar Altimeter," Document 633-420, JPL, Pasadena, CA, 1989.
[50] "TOPEX project radar altimeter development requirements and specifications," NASA Goddard Space Flight Center, Wallops Flight Facility Internal Publications, WFF-672-85-004, Aug. 25, 1988.

Paul C. Marth received the B.E.S. and M.E.S. degrees in electrical engineering from the Johns Hopkins University in 1961 and 1968, respectively.

He joined APL in 1961 as a specialist in digital design in the Space Department. Since 1974, he has been involved in numerous system design problems, including the SEASAT-A remote sensing satellite, the GPSPAC spaceborne GPS receiver, and the N-Ross radar altimeter. His recent work includes serving as system Engineer for the GEOSAT and TOPEX radar altimeters.

Mr. Marth is a member of Tau Beta Pi and IEEE.

J. Robert Jensen received the B.A. degree from Cornell College in Mt. Vernon, IA, in 1973 and the Ph.D. degree in physical chemistry from the University of Wisconsin, Madison, in 1978.

He joined APL in 1978 and has been involved in numerous non-acoustic detection problems, principally involving radar. His recent work has focused on modeling the properties of microwave backscatter from the ocean surface and applying these models to radar altimetry, synthetic aperture radar imaging, delta-k radar processing, and other means of inferring ocean characteristics from radar data.

Charles C. Kilgus received the B.S. degree in electrical engineering from Drexel Institute of Technology in 1964 and the M.S.E. and Ph.D. degrees from The Johns Hopkins University in 1968 and 1970, respectively, specializing in communications theory.

Since joining APL in 1964, he has worked in the Space Department on various antenna, communications, and system design projects including Transit, Dodge, GEOS-B and -C, SEASAT, GEOSAT, and TOPEX/POSEIDON. Dr. Kilgus is currently a principal staff engineer and program manager in the Space Department.

James A. Perschy received the B.S.E.E. degree from the George Washington University in 1958 and the M.S. degree in physics from the University of Maryland in 1965.

In 1958, he joined APL, where he designed the data handling system and memories for the early Navy navigation satellites and the general-purpose computer for the Tip and Nova series. His designs include a sonar beam former and intercept receiver, a loran receiver/navigator, and a digital communications network. He has received seven patents in digital processing. A second supervisor in the Digital Flight Systems Group, he is currently leading the TOPEX signal processor effort and is a consultant to GEOSAT Follow-On.

John L. MacArthur was born in Columbus, OH, and received the B.S. degree in electrical engineering from the Catholic University of America in 1951 and the M.S. degree in electrical engineering from the University of Maryland in 1959.

He joined APL in 1957 and was appointed to the principal professional staff in 1972. His primary specialty is radar system design. After joining the Space Department in 1974, he served as Project Scientist for radar altimeter development on the SEASAT program and is currently performing a similar role in the GEOSAT, TOPEX, and GEOSAT Follow-On spaceborne altimeter programs.

David W. Hancock was born in Stockton, MD, in 1946. He received the B.S. degree in mathematics from East Carolina University, Greenville, NC, in 1970.

In 1964, he joined NASA Wallops Flight Center, Wallops Island, VA, as an electronic technician apprentice and completed its requirements in 1968. Since 1970 he has been at the NASA Goddard Space Flight Center's Wallops Island Facility. He has worked on the real-time computer control for radar and laser altimeters and algorithms for ground processing of the altimeter data. He is presently a senior scientist for the TOPEX/NASA radar altimeter.

George S. Hayne (M'73) was born in 1937 in Ann Arbor, MI. He received the B.A. degree in physics in 1958 from Kalamazoo College, Kalamazoo, MI, and the Ph.D. degree in physics in 1966 from Yale University, New Haven, CT. He did postdoctoral work in physics at Duke University, Durham, NC.

He held staff positions at the Research Triangle Institute, Research Triangle Park, NC, and at Applied Science Associates, Apex, NC. Since 1980, he has been with the NASA Goddard Space Flight Center's Wallops Island Facility at Wallops Island, VA. His current technical interests are in the general area of remote sensing of planetary surfaces, and the specific areas of radar altimetry and its associated data correction and processing.

Dr. Hayne is a member of AGU and of Sigma Xi.

Craig L. Purdy was born in Chincoteague, VA, in 1947. He received the B.S. degree in electrical engineering from Virginia Polytechnic Institute in 1970.

Since 1970 he has been with the NASA Goddard Space Flight Center's Wallops Island Facility, Wallops Island, VA, in the Radar and Optical Systems Section. He was a system engineer on the Skylab S-193 Radar Altimeter, the Experiment Manager on the GEOS-3 Radar Altimeter, the Systems Engineer on the SEASAT Radar Altimeter, and is presently the Sensor Development Manager for the TOPEX/NASA Radar Altimeter.

Laurence C. Rossi was born in Harrison Township, PA, in 1942. He received the B.S. degree in electronics engineering from Northrup Institute of Technology in 1962.

Since 1963, he has been with the NASA Goddard Space Flight Center, Wallops Flight Facility, Wallops Island, VA, in the Laboratory for Hydrospheric Processes, Observational Sciences Branch. He was Project Manager for the Geodetic Earth Orbiting Satellite (GEOS)-3 which was launched in 1975 and successfully completed 3 years of operations. He is currently the NASA Instrument Manager for the Ocean Topography Experiment (TOPEX) Radar Altimeter). He is a member of the American Geophysical Union, Oceans Sciences (75), and the Oceanography Society (88).

Chester J. Koblinsky graduated in 1971 from Reed College in Portland, OR with a B.A. in physics. He received the Ph.D. degree in physical oceanography from Oregon State University in 1979.

He is the head of the Oceans and Ice Branch at the Goddard Space Flight Center in Greenbelt, MD. He worked in the Geodynamics branch at Goddard for eight years starting in 1987 after 4 years as a research oceanographer at Scripps Institution of Oceanography. At Goddard, Dr. Koblinsky is the principal investigator of a TOPEX/POSEIDON science team which is conducting investigations on the general ocean circulation and the structure of the geoid. He is also a team leader for ERS-1 altimeter and scatterometer investigations on ocean circulation. In addition, he serves as the instrument scientist for the Earth Observing System altimeter mission. He has published over 40 papers on physical oceanography and ocean remote sensing.

Dr. Koblinsky was awarded the NASA Medal for Exceptional Scientific Achievement in 1990 for his work on ocean circulation utilizing satellite altimetry. He is a member of AGU, the American Meteorological Society, the Oceanography Society, and a former member of IEEE and the Geoscience and Remote Sensing Society.